Available online at www.sciencedirect.com
ScienceDirect
Forest Ecology and Management 255 (2008) 2602–2616
Forest Ecology and Management
www.elsevier.com/locate/foreco

Spatial partitioning of biomass and diversity in a lowland Bolivian forest: Linking field and remote sensing measurements

Eben N. Broadbent [a,b,*], Gregory P. Asner [a], Marielos Peña-Claros [c,d], Michael Palace [e], Marlene Soriano [c]

[a] Department of Global Ecology, Carnegie Institution, 260 Panama Street, Stanford, CA 94305, USA
[b] Department of Biological Sciences, Stanford University, Stanford, CA 94305, USA
[c] Instituto Boliviano de Investigación Forestal, P.O. Box 6204, Santa Cruz de la Sierra, Bolivia
[d] Forest Ecology and Forest Management Group, Wageningen University, P.O. Box 47, Wageningen 6700 AA, The Netherlands
[e] Complex Systems Research Center, Morse Hall, University of New Hampshire, Durham, NH 03824, USA

Received 31 July 2007; received in revised form 9 January 2008; accepted 9 January 2008

Abstract

Large-scale inventories of forest biomass and structure are necessary for both understanding carbon dynamics and conserving biodiversity. High-resolution satellite imagery is starting to enable structural analysis of tropical forests over large areas, but we lack an understanding of how tropical forest biomass links to remote sensing. We quantified the spatial distribution of biomass and tree species diversity over 4 ha in a Bolivian lowland moist tropical forest, and then linked our field measurements to high-resolution Quickbird satellite imagery. Our field measurements showed that emergent and canopy dominant trees, being those directly visible from nadir remote sensors, comprised the highest diversity of tree species, represented 86% of all tree species found in our study plots, and contained the majority of forest biomass. Emergent trees obscured 1–15 trees with trunk diameters (at 1.3 m, diameter at breast height (DBH)) $\geq$20 cm, thus hiding 30–50% of forest biomass from nadir viewing. Allometric equations were developed to link remotely visible crown features to stand parameters, showing that the maximum tree crown length explains 50–70% of the individual tree biomass. We then developed correction equations to derive aboveground forest biomass, basal area, and tree density from tree crowns visible to nadir satellites. We applied an automated tree crown delineation procedure to a high-resolution panchromatic Quickbird image of our study area, which showed promise for identification of forest biomass at community scales, but which also highlighted the difficulties of remotely sensing forest structure at the individual tree level.

Keywords: Amazon; Biomass; Bolivia; Tree crown delineation; Tropical forest; Quickbird satellite images

1. Introduction

The spatial partitioning of biomass in tropical forests largely results from high species diversity, different survival strategies, and varying disturbance regimes (Whitmore, 1978). This partitioning plays a role in determining future forest structure, and thus biomass partitioning, by altering micro-climatic and biogeochemical conditions, and thus forest community dynamics (Brokaw, 1985; Kuppers, 1989; Whitmore, 1989; Guariguata et al., 1997). The resultant three-dimensional structure and composition of a forest partially defines its utility for human activities and the capacity of the forest to support animal and plant populations (Hansen et al., 1991). Forest structure also mediates carbon sequestration following both natural and anthropogenic disturbances (Cummings et al., 2002; Vieira et al., 2004). Few studies, however, have quantified how biomass is spatially distributed within tropical forests due to the complexity of multi-tiered canopies, large differences in tree diameter and height, and their generally large stature (Asner et al., 2002). A more accurate understanding of the three-dimensional partitioning of forest biomass would enhance our understanding of terrestrial carbon dynamics and provide insights into potential impacts of forest degradation (Phillips et al., 1998; Chambers et al., 2000; Keller et al., 2001).

Future approaches for rapid, cost-effective, fine-scale quantification of forest structure and diversity over large areas

* Corresponding author at: Department of Biological Sciences, Stanford University, Stanford, CA 94305, USA. Tel.: +1 650 704 2065; fax: +1 650 462 5968.
E-mail address: eben@stanford.edu (E.N. Broadbent).

0378-1127/$ – see front matter © 2008 Elsevier B.V. All rights reserved.
doi:10.1016/j.foreco.2008.01.044

will likely rely on remotely sensed data. Excellent results are being derived from LiDAR (light detection and ranging) systems (Drake et al., 2002), and headway is being made on both manual and automated interpretation of high-resolution optical satellite imagery (Asner et al., 2002; Clark et al., 2004; Palace et al., 2008). However, a current limitation on all nadir-viewing sensors is imposed by the spatial arrangement of forest canopies, in particular where larger diameter and taller canopy trees overtop numerous smaller individuals. Although the quantification of viewable versus total forest stems from nadir perspectives would be valuable for correction of remotely sensed data, no study has yet provided the integrated, detailed vertical and horizontal spatial analyses necessary to calibrate the relationship between remote sensing and tropical forest structure. Likewise, few studies have quantified the spatial distribution of tree species diversity as is relevant to nadir-viewing remote sensors. A better understanding of tree species spatial distribution and visibility to nadir sensors is relevant both to improving biomass estimations through better tree crown delineations and to forest management and biodiversity conservation.

In this study, we quantified the structural partitioning of forest biomass and species diversity in a tropical moist forest in lowland Bolivia by developing high-resolution, three-dimensional spatial maps of trees and their structural attributes within four 1-ha study plots. Principal questions addressed in our study were: (1) how is biomass distributed throughout the forest and by both tree-diameter and crown-position classes? (2) how is tree diversity distributed through these same classes? (3) how are tree stems and crowns spatially distributed throughout the stand? and (4) what implications do these results have for remote sensing of fine-scale forest structure and biomass?

2. Methods

2.1. Study area

This study was conducted in the timber concession of Agroindustria Forestal La Chonta Ltda., which encompasses 100,000 ha of forest in the Guarayos province of the Department of Santa Cruz, Bolivia (15°47′S, 62°55′W; also see Fig. 3). The elevation at the site is 400–600 m above sea level, with mildly undulating topography. Geologically, it is a continuation of the Brazilian Shield with moderately fertile inceptisols and patches of black anthrosols throughout the concession (Calla, 2003; Paz, 2003). Vegetation is classified as moist tropical semi-deciduous forest and has a biomass range of 73–190 Mg/ha (Dauber et al., 2000). For trees ≥10 cm in diameter (at 1.3 m diameter at breast height; DBH) the average tree density is 368 trees/ha, with mean basal area of 19.7 m^2/ha, mean canopy height of 25 m, and on average 59 species/ha (all data for trees ≥10 cm in diameter at 1.3 m height from the ground (DBH); Peña-Claros et al., 2008). The average annual temperature is 25 °C. Mean annual precipitation in the region is ∼1580 mm, with 4 months receiving <100 mm (May–September) and 1 month (July) during which potential

Table 1
Abundance and structural variables (mean (±S.E.)) for trees ≥20 cm in DBH in the four 1-ha plots included in this study

	Study plot			
	1	2	3	4
Variable				
Tree abundance (≥20 cm DBH)	119	66	162	184
Richness	32	31	26	37
Diversity[a]	2.76	3.15	1.79	2.39
Mean (±S.E.) percentage of tree stems in each crown exposure class				
Crown exposure 5	31 (0.26)	14 (0.21)	27 (0.17)	36 (0.20)
Crown exposure 4	18 (0.15)	13 (0.20)	30 (0.19)	48 (0.26)
Crown exposure 3	22 (0.19)	27 (0.41)	33 (0.20)	50 (0.27)
Crown exposure 2	34 (0.29)	10 (0.15)	49 (0.30)	36 (0.20)
Crown exposure 1	14 (0.12)	2 (0.03)	23 (0.14)	14 (0.08)
Structural variables mean (±S.E.) and Tukey's HSD post hoc analyses results[a]				
Basal area (m^2/ha)	15.21	8.92	25.52	27.04
Average DBH	35.4 (2.0)	37.0 (2.6)	38.3 (1.7)	37.3 (1.6)
Branch height	9.7 (0.3)	8.6 (0.5)	9.7 (0.3)	9.8 (0.3)
Crown base height	12.8 (0.4)	12.3 (0.6)	13.8 (0.4)	13.3 (0.3)
Total tree height	19.7 (0.7)	19.5 (0.9)	22.7 (0.6)	21.5 (0.6)
Crown length	9.9 (0.5)	11.3 (0.8)	11.2 (0.5)	11.5 (0.5)
Crown width	6.9 (0.5)	8.0 (0.7)	7.9 (0.5)	8.0 (0.4)
Crown depth	6.1 (0.3)	6.6 (0.5)	8.0 (0.3)	7.3 (0.3)
Crown area	77.9 (13.8)	96.8 (20.3)	96.8 (13.1)	91.8 (11.1)
Crown volume	496.2 (130.1)	702.1 (258.0)	801.7 (167.8)	639.9 (127.4)
Crowns detected remotely[b]	64	186	58	62

Stem abundance per crown exposure class is also provided.
[a] Shannon–Weiner diversity index.
[b] Number of individual tree crowns identified using automated delineation of the panchromatic Quickbird satellite image.

evapotranspiration exceeds rainfall (Peña-Claros, unpublished data). Seasonally deciduous and semi-deciduous forests like La Chonta provide about 45% of Bolivia's timber and encompass about 35% of the area designated for forest management (Superintendencia Forestal, 2002). The region is vulnerable to wildfires, and 30% of the concession was burned in 1995 (Cordero, 2000; Gould et al., 2002) and 2004 (C. Pinto, personal communication).

Four 100 m × 100 m (1 ha) and one 100 m × 50 m study plots were established within two ~27-ha stands belonging to the Long-term Silvicultural Research Program (LTSRP), established by the Instituto Boliviano de Investigación Forestal in different forest types within Bolivia (IBIF; more information available online at www.ibifbolivia.org.bo). The study plots had not been logged or burned in recent history. Initial plot locations were randomly selected, but then shifted so the edges of the 1-ha plots fell on established trails of the LTSRP plots (located every 50 m within the 450 m × 600 m LTSRP plots). All trees ≥20 cm in DBH within the 1-ha study plots had been mapped previously to a Cartesian coordinate system by IBIF technicians and identified to species level. The most abundant species in the plots were *Pseudolmedia laevis* (Moraceae), *Ampelocera ruizii* (Ulmaceae) and *Terminalia oblonga* (Combretaceae). The four 1-ha plots were used for all spatial analyses, while data from the fifth 0.5 ha plot was used to increase the sample size for development of allometric equations. Descriptive statistics of the four study plots is provided in Table 1.

2.2. Forest structure

Field data were collected from December 2005 through February 2006. For each tree, we measured the DBH, total tree height (from base of the trunk to the highest branch or foliage), height to the first large branch (defined as the first major trunk bifurcation), base to the crown (defined as the base of a sphere containing greater than 75% of the trees foliage), crown maximum length (m) and width (m), and horizontal offset (distance (m) and azimuth) of the crown center from the trunk location. For each tree, we also defined crown exposure using a five-point scale (Clark and Clark, 1992) in which 1 = no direct light or low amount of lateral light, 2 = intermediate or high amount of lateral light, 3 = vertical light in part of the crown, 4 = vertical light in the whole crown, and 5 = exposed crown with direct light coming from all directions.

The tree height, height to the first large branch, and crown base were estimated by two separate observers in 0.5 m increments. To correct for observer error, the observer-estimated heights (referred to as *estimated heights*) of 106 trees were regressed against height measurements made on the same trees using a handheld laser range finder (referred to as *laser heights*; Impulse-200LR, Laser Technology Inc., Englewood, Colorado). The estimated height to the first branch showed a significant linear relationship with that of the laser range finder (estimated height = 1.48 + 0.85 × laser height, $r^2 = 0.88$, $p < 0.0001$), and the estimated tree height had a significant linear relationship with laser total tree height (estimated total height = 0.745 + 0.89 × laser total height; $r^2 = 0.90$, $p < 0.0001$). As the laser rangefinder was available only for the first portion of the field campaign, all height data collected thereafter were corrected using the regression equations described above. To ensure against gradual changes in estimated height accuracy during data collection, we calibrated our height estimates each morning prior to fieldwork by estimating the heights of 10–15 trees previously measured with the laser range finder. All subsequent statistical and descriptive analyses were conducted on the corrected height data.

Crown length (transect of maximal distance) and width (perpendicular distance) were measured in the field using a 50-m measuring tape. A clinometer was used to identify the location directly beneath the outermost edge of each tree crown. Error due to topography was minimized by holding the tape as horizontal as possible prior to recording the crown dimensions. Canopy center offset from the trunk was assessed by measuring the distance from the crown center point to the trunk base. Crown area was calculated assuming an oval shape with maximum crown length (L) and the perpendicular width (W) being the explanatory axes. Crown volume was calculated assuming a perfect spherical ellipsoid with width (W), length (L) and depth (D) being the three explanatory variables; crown depth was calculated as the difference between maximum tree height and crown base.

Forest biomass was calculated using six equations available in the literature (Brown, 1997; Araujo et al., 1999; Carvalho et al., 1988; Chave et al., 2005; see Appendix A for equations). Two biomass equations derived from Chave et al. (2005) required species-specific wood density values, which were largely unavailable at the species level. Therefore we used wood density at the finest taxonomic resolution available via a web-based wood density database (http://www.worldagroforestrycentre.org/sea/Products/AFDbases/wd), which allowed us to obtain wood density data at the family, genus and species level for 52, 40 and 8% of the tree individuals in our study plots, respectively. It has been shown that wood density information at the order, family, genus and species levels contributed an additional 12.1, 13.3, 45.6 and 29.6%, respectively, of explanatory power over wood density variation (Baker et al., 2004; Slik, 2006). Consequently, we believe that our biomass estimates, which included wood density, provided a more accurate representation of tree biomass than those relying on DBH and height alone.

Separate one-way analyses of variance (ANOVA) among the five crown position classes were carried out for all structural parameters, followed by Tukey's HSD post hoc analyses when significant differences were found. All variables were log transformed prior to analysis to meet assumptions of data distribution normality. Optimal bi- and multi-variate power regression models were identified between all structural parameters using TableCurve 2D and 3D (Versions 5.01 and 4.0, respectively, Point Richmond, CA, USA: Systat, Inc.).

2.3. Forest composition

Species richness, abundance, diversity, and basal area (m^2/ha) were calculated for the four study plots, the five crown position classes, and for each DBH category. Diversity differences between the DBH and crown exposure classes were compared using the Shannon–Weiner diversity index. Changes in species composition between the crown exposure classes were compared using Sorensen's similarity index.

2.4. Spatial analyses

The Cartesian coordinate arrays from study plots 1–2 and 3–4 were geo-referenced to 22 and 17 differentially corrected GPS (Geographic Positioning System; Leica GS-50+, Leica Geosystems, St. Gallen, Switzerland) points, respectively. The grid points were converted to Universal Transverse Mercator (UTM; zone 20 South, datum WGS 1984) using linear regression. Root mean square errors (RMSE) for the regression equations were 5.6 and 6.1 m, respectively. Fine scale geo-referenced topographic data of the LTSRP plots was obtained from the Instituto Boliviano de Investigación Forestal (Vroomans, 2003), which was used to correct the vertical positioning of tree crowns prior to spatial analyses.

Following geo-rectification, maps of tree crown and trunk locations were created in a Geographic Information System (GIS; ArcInfo, Redlands, CA, USA). This process enabled vertical and horizontal spatial analysis of tree distributions and crown positions. The average distance between tree individuals within each of the five crown exposure classes was calculated using a linear least distance approach. Tree density was calculated for each crown exposure class and all classes together by first dividing each study plot into 5 m × 5 m subsections and then counting all tree stems within 10 m of each subsection and dividing the number of tree stems by the search area (490 m^2). We then calculated histograms of the density distributions within each plot, ranging from 0 to 0.02 stems/m^2, for each crown exposure class. Density distributions were compared among crown exposure categories using separate one-way ANOVA ($n = 4$ plots).

The mean number of trees located beneath individual tree crowns was calculated separately for each DBH and crown exposure class—henceforth referred to as *obscured trees*. Correlations between crown dimensions and the number of obscured trees were used to develop correction equations between nadir-visible trees and those identified and mapped in the field. These equations were developed for trees in crown exposure classes 3–5 only because the other exposure classes, by definition, were not visible to nadir-viewing optical remote sensors. We refer to biomass derived using the equation corrected for obscured tree stems as the *corrected biomass*.

Field geo-referenced data of each plot were used to link the plot location to a Quickbird image acquired of our study area on 15 September 2005 at 4:37 pm GMT (11:00 am local time). The image acquisition angle was $<5^\circ$ from nadir. The image was acquired at a resolution of 0.4 m panchromatic and 1.4 m multi-spectral. The image was geo-rectified using a first-degree linear regression model to 62 differentially corrected ground control points clustered around the study plots. The root mean square (RMS) error of the warp was 3.5 m, and the final projection was Universal Transverse Mercator (UTM; zone 20 South, datum WGS 1984).

Individual tree crowns were delineated in the panchromatic Quickbird imagery using an automated procedure developed by Palace et al. (2008). The procedure combines iterative detection of local maxima values with a 360 directional linear search algorithm to identify inter-pixel change events in the panchromatic image exceeding a defined threshold. No calibration to field data was conducted prior to image processing to assess the utility of the approach to areas not having extensive field data. The original algorithm was developed using field data from Cauaxi, Para, Brazil (Palace et al., 2008), and was previously applied successfully at seven sites spanning the Amazon basin, indicating the robustness of the algorithm to provide landscape-level estimates of vegetation structure. However, this analysis used community-wide distribution comparisons rather than tree-to-tree comparisons, as we conducted in this study. As it is possible to achieve similar DBH distributions between RS and field assessments for the incorrect reason (e.g., some over-estimates compensated by some underestimates) we seek to further elucidate the forest DBH distributions and resultant standing biomass estimates from RS using the spatially explicit analysis presented in this study.

Automated delineations of tree crowns were made as both polygons (incorporating the 360 search transects) and circles (using the average of the longest opposite ordinal transects as the radius). Individual tree crown area calculated from these methods was input into the allometric relationship between field-derived crown area and DBH to calculate remotely sensed DBH distributions over the study area. Both corrected and raw nadir-visible biomass data were calculated using the allometric crown area-to-biomass equations illustrated in Fig. 5. Crown area, DBH and biomass results were categorized to resolutions of 25 m^2, 10 cm and 1 Mg, respectively, based on a visual inspection of data distributions. Kolmogorov–Smirnov analyses were used to compare distributions of categorized tree abundances. Direct remote sensing to field comparison at the tree scale were conducted by randomly selecting tree individuals from crown exposure classes 3, 4 and 5, and then quantifying the number of remote sensing detections having their center point within the field-delineated tree crown. Remote sensing biomass calculations at the tree scale were made by inputting the summed area of all automated detections within that tree's crown into the corrected biomass. Paired *t*-tests and linear regressions were used to compare field derived individual crown area, DBH and biomass with the remote sensing polygon approach.

3. Results

3.1. Forest structure

The majority of the trees within the study plots had DBH values of 20–29 cm (Table 2). Basal area remained similar

Table 2
Abundance, basal area and biomass per DBH classes present throughout the four 1-ha study plots

DBH (cm)	Abundance (stems/ha)	Basal area (m^2/ha)	Biomass (±S.E.) (kg/ha)[a]	Richness (4 ha)	Diversity (4 ha)[b]
20 ≤ 29	61.75	2.92	26.69 (5.38)	41	2.24
30 ≤ 39	30.00	2.80	29 (3.96)	25	2.04
40 ≤ 49	13.25	2.12	23.31 (3.03)	22	2.46
50 ≤ 59	9.25	2.10	24.7 (3.01)	21	2.75
60 ≤ 69	5.50	1.82	23.08 (2.75)	13	2.29
70 ≤ 79	1.75	0.73	9.62 (1.25)	5	1.48
80 ≤ 89	1.50	0.84	11.69 (1.64)	5	1.56
90 ≤ 99	1.50	1.02	14.06 (2.54)	4	1.33
100 ≤ 109	0.75	0.59	8.6 (1.44)	3	1.10
110 ≤ 119	1.50	1.52	22.31 (4.55)	5	1.56
120 ≤ 129	1.25	1.46	22.01 (4.64)	3	1.05
130 ≤ 139	0.25	0.36	6.3 (1.18)	1	0.00
≥140	0.25	0.79	15.22 (3.69)	1	0.00

[a] Mean and standard error of the six biomass equations described in the methods section.
[b] Shannon–Weiner diversity index.

among DBH classes, showing only a 50% reduction as compared to the tenfold reduction in tree abundance and biomass. Across the four plots, there were more trees in the crown exposure class 3 (25%; trees receiving partially vertical light), followed by canopy position 5 (20%; emergent trees), while few trees (10%) had crowns located in crown exposure class 1 (Table 3). Basal area across our study plots was dominated by tree individuals in crown exposure class 5, which exceeded the summed basal area of all individuals in the other four crown exposure classes (Table 3).

Emergent trees (exposure class 5) are represented by trees belonging to a wider range of DBH classes, as indicated by the greater standard error value, than any other crown exposure class, and the percentage of trees belonging to crown exposure class 5 is larger as trees increase in size (Fig. 1). The majority of forest biomass was stored in trees in

Table 3
Forest structure and crown characteristics per crown exposure class

Variable	Crown exposure class				
	1 (Understory)	2	3	4	5 (Emergent)
Forest structure					
Tree density (#/ha)	53	129	132	109	108
Richness	14	26	27	26	35
Total species represented (%)	24	44	46	44	59
Diversity[a]	1.501	1.891	2.291	2.198	3.063
Basal area (m^2/ha)	0.58	2.01	2.75	3.91	9.92
DBH (cm)***	23.2 (0.7) D	27.0 (0.7) D	30.8 (0.9) C	40.3 (1.4) B	60.8 (3.0) A
Biomass ± S.E. (kg/ha)[b]	5.92 (1.98)	20.88 (5.34)	29.8 (7.2)	46.03 (9.45)	138.9 (38.53)
Crown structure					
Branch height (m)***	7.8 (0.4) C	8.2 (0.3) C	8.0 (0.3) C	10.8 (0.4) B	12.7 (0.4) A
Total tree height (m)***	16.8 (0.6) C	17.8 (0.4) C	18.0 (0.5) C	23.0 (0.6) B	29.7 (0.8) A
Crown length (m)***	8.2 (0.4) C	8.6 (0.3) C	9.7 (0.4) C	11.3 (0.4) B	16.8 (0.9) A
Crown width (m)***	5.5 (0.3) C	5.8 (0.2) C	6.5 (0.3) C	7.6 (0.3) B	12.7 (0.9) A
Crown area (m^2)***	38.9 (3.8) C	44.1 (3.5) C	57.9 (5.7) C	75.4 (5.4) B	228.0 (28.4) A
Crown depth (m)***	5.7 (0.3) C	5.7 (0.2) C	6.0 (0.3) C	7.7 (0.3) B	10.5 (0.5) A
Crown volume (m^3)***	160.9 (20.9) C	188.8 (21.6) C	310.6 (67.6) C	437.1 (47.6) B	2138.5 (346.6) A
Max (min) length (m)	16.3 (3.5)	20.5 (1.5)	28.4 (2.0)	24.4 (4.0)	48.5 (2.7)
Max (min) width (m)	12.0 (1.0)	19.4 (1.0)	25.0 (1.0)	18.6 (1.4)	40.0 (2.0)
Max (min) area (m^2)	146 (5.5)	312 (1.2)	558 (3.5)	357 (6.3)	1523 (4.7)
Spatial distribution					
Tree separation ± S.E. (m)[c]	27.32 (11.54)	13.27 (2.99)	10.97 (1.22)	14.19 (3.46)	10.59 (0.87)
Nadir visible crown area ± S.E. (%)[d]	20.14 (12.92)	16.54 (2.49)	53.91 (7.59)	60.74 (5.55)	100 (0)

Data given are mean (±S.E.). When applicable, results of one-way ANOVA are given testing differences for the different variables among crown exposure classes. Different letters indicate significant differences; p-values: *$p < 0.05$, **$p < 0.01$, ***$p < 0.001$.
[a] Shannon–Weiner diversity index.
[b] Mean and standard error of the six biomass equations described in the methods section.
[c] Mean linear distance and standard error separating tree individuals across each of the four study plots.
[d] Mean and standard error crown area visible from a nadir perspective for all trees in each crown exposure class.

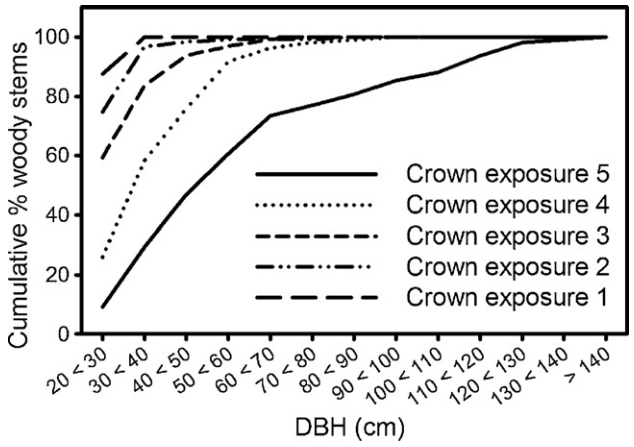

Fig. 1. Cumulative percentage of total woody stems ≥20 cm in diameter (DBH) within individual crown exposure classes along a DBH gradient. Crown exposure classes 1–5 are completely shaded to fully exposed tree crowns.

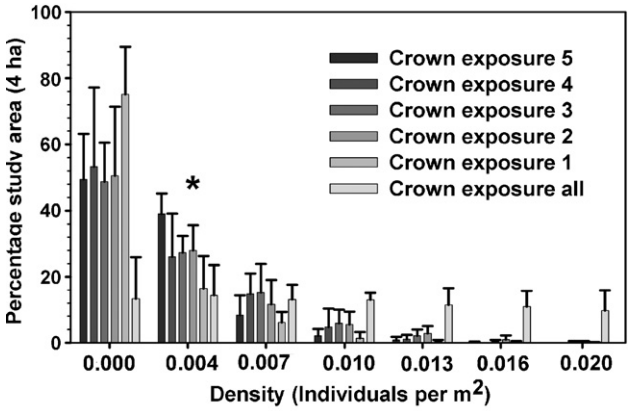

Fig. 2. Tree stem density by crown exposure class and for all exposure classes combined. Error bars represent standard deviation of the mean among the four 1-ha study plots. The asterisk represents significant differences among crown positions ($p < 0.05$).

crown exposure class 4 and 5, in particular exposure class 5 stored 139 Mg/ha, which was equal to the biomass found in all other crown positions combined (Table 3). Mean crown area and crown length of emergent trees was 228 m^2 and 17 m, respectively, while these variables for exposure class 4 were only 75 m^2 and 11 m, respectively. The maximum length of crowns of emergent trees was double that of crown position 4, though only smaller decreases were found from crown position 1–4. Maximum crown area increased from 146 to 357 to 1523 m^2 in crown exposure classes 1, 4 and 5, respectively (Table 3). The simplest biomass equations, which included only DBH (Appendix A, Eqs. A–D), produced lower biomass estimates than those incorporating wood density and tree height (Appendix A, Eqs. E and F), resulting in twofold differences in derived biomass.

The 216 allometric equations between forest structural variables are presented in Appendix B. A subset of these equations was chosen based on their explanatory power and utility for linking nadir top-of-canopy visible parameters to field measurements which are provided in Table 4. All allometric equations presented in Table 4, with the exception of DBH in crown exposure class 1, had p-values <0.001. For emergent trees, crown length and crown area had the greatest explanatory power of tree DBH ($r^2 = 0.74$ and 0.73, respectively).

3.2. Forest composition

A total of 59 tree species were found within our study area, dominated by the tree species *P. laevis* (Moraceae). Although tree abundance (≥20 cm DBH) varied threefold among study parcels, tree species richness varied far less with minimum and maximum species numbers of 26 and 37 found in study plots 3 and 4, respectively (Table 1). Species richness and stem abundance, 41 and 62, respectively, were greatest in DBH category 20–29 cm, and decreased rapidly to 25 and 30, respectively, in DBH category 30–39 cm. DBH categories greater than 70 cm were composed of fewer than five species. Species diversity followed a similar trend, but peaked in DBH

Table 4
Allometric relationships between crown width (W), length (L), and area (A) and tree DBH and tree total height (H)

Variable	Crown exposure class	Crown width (m)	Crown length (m)	Crown area (m^2)
DBH (cm)	5	$=21.96 + 3.02 \times W(0.68)$***	$=10.55 + 2.97 \times L(0.74)$***	$=16.35 + 3.44 \times A^{0.5}(0.73)$***
	4	$=24.10 + 0.10 \times W(0.58)$***	$=24.06 + 0.10 \times L^2(0.58)$***	$=31.43 + 0.009 \times A^{1.5}(0.65)$***
	3	$=22.79 + 0.07 \times W(0.51)$***	$=11.60 + 1.94 \times L(0.47)$***	$=23.91 + 0.11 \times A(0.43)$***
	2	$=4.85 + 0.0004 \times W(0.49)$***	$=15.91 + 1.26 \times L(0.27)$***	$=24.84 + 0.001 \times A^2(0.53)$***
	1	NS	$=19.12 + 0.47 \times L(0.08)$*	NS
	All	$=17.0 + 0.48 \times W(0.68)$***	$=4.13 + 2.92 \times L(0.65)$***	$=7.62 + 3.60 \times A^{0.5}(0.66)$***
Tree height (m)	5	$=12.53 + 5.06 \times W^{0.5}(0.46)$***	$=18.56 + 0.66 \times L(0.50)$***	$=19.94 + 0.75 \times A^{0.5}(0.48)$***
	4	$=15.98 \times 0.97 \times W(0.23)$***	$=14.38 + 0.77 \times L(0.27)$***	$=14.57 + 1.07 \times A^{0.5}(0.27)$***
	3	$=12.22 + 0.97 \times W(0.29)$***	$=10.94 + 0.76 \times L(0.30)$***	$=11.15 + 1.05 \times A^{0.5}(0.32)$***
	2	$=14.37 + 0.58 \times W(0.10)$***	$=12.22 + 0.63 \times L(0.19)$***	$=15.59 + 0.48 \times A(0.16)$***
	1	$=12.12 + 0.95 \times W(0.22)$***	NS	NS
	All	$=14.05 + 0.96 \times W(0.41)$***	$=11.57 + 0.89 \times L(0.46)$***	$=12.61 + 1.09 \times A(0.45)$***

For sample sizes in each crown exposure class refer to Table 3. r^2 values are provided in parenthesis and p-values are coded as follows: *$p < 0.05$, ***$p < 0.001$; NS = non-significant and are provided following each equation.

Table 5
Sorensen's index of species composition similarity between crown position classes

	Crown exposure class			
	1	2	3	4
2	0.45	1		
3	0.44	0.57	1	
4	0.25	0.62	0.53	1
5	0.2	0.43	0.45	0.59

category 50–59 cm (Table 2). For crown exposure classes, the highest species richness and diversity were found in emergent trees (35 spp.), followed by exposure class 3 (27 spp.; Table 3). Species composition was the least similar between crown exposure class 1 and 5, while species compositions were more similar for closer exposure classes (Table 5). The majority of tree species were represented within the emergent crown exposure class (Table 5). Cumulatively, from emergent through understory trees (classes 5, 5-4, 5-3, 5-2 and 5-1, respectively), we found that 59, 73, 86, 95 and 100% of all tree species were represented.

3.3. Spatial analyses

Tree individuals in crown exposure class 1 occurred approximately 27 m apart, while those in crown exposure class 5 occurred an average of 11 m apart (Table 3). Fig. 2 illustrates the distribution of tree stem density by crown position. The two-way ANOVA showed significant differ-

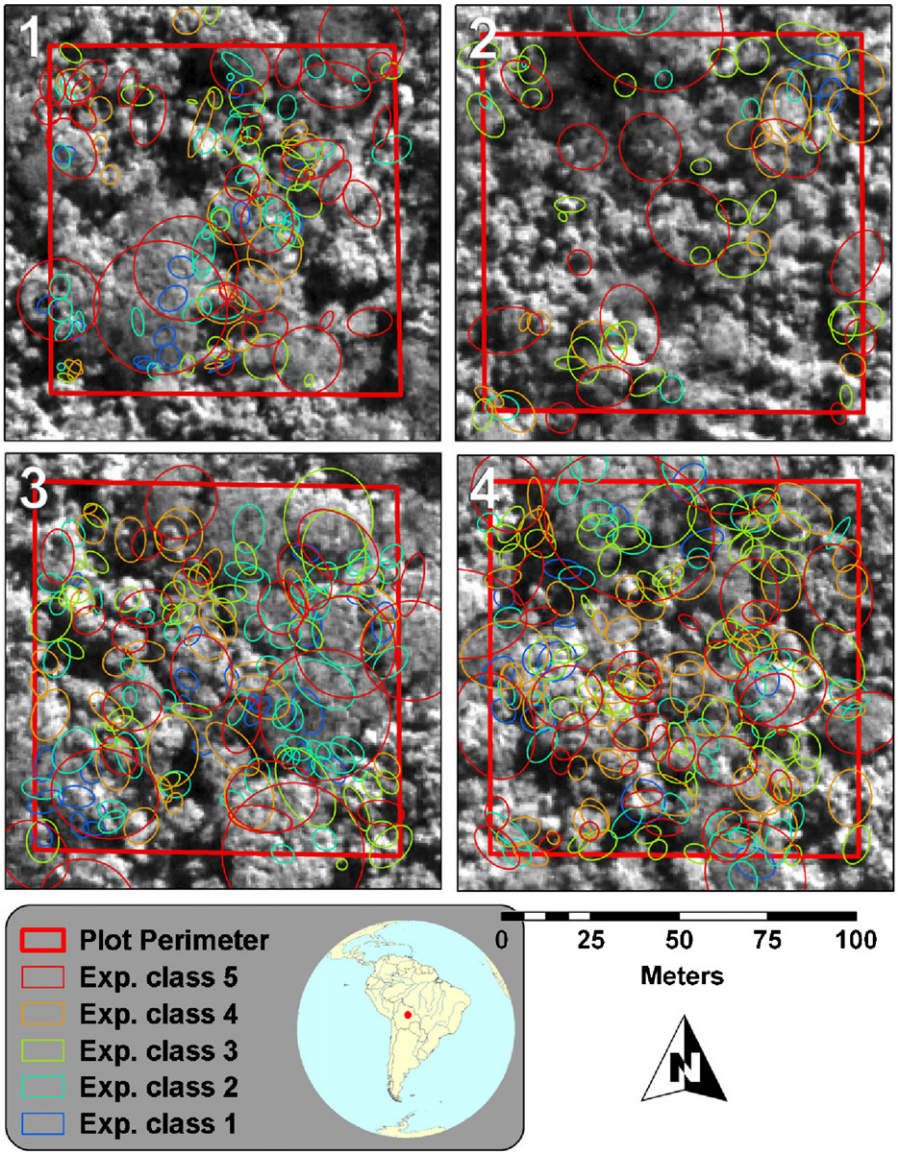

Fig. 3. Field geolocated tree crowns (DBH ≥ 20 cm) in crown exposure classes 1 (shaded understory) through 5 (emergent) for the four study plots. Crown delineations are overlaid on the panchromatic Quickbird satellite image. Areas within each plot but outside delineated tree crowns represent crowns of trees not meeting our DBH ≥ 20 cm threshold.

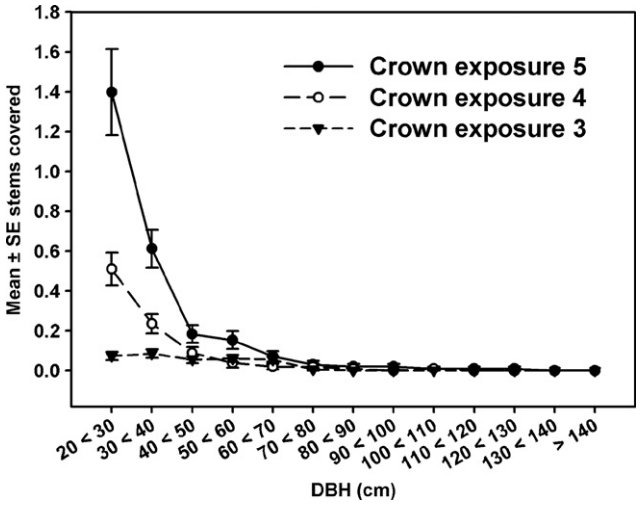

Fig. 4. Mean number of stems covered by trees belonging to crown exposure class 5, 4 and 3. Error bars represent standard errors of the mean.

ences between tree densities in the five crown exposure classes at the 0.003 density class, with crown position 5 having the greatest abundance at this density. There were no significant differences among the five crown exposure classes at the other densities; although a trend was observed with the greatest area of zero stem density being found in crown exposure class 1.

A map of crown positions generated from the field data is provided in Fig. 3. The majority of obscured tree stems were located within smaller DBH classes (Fig. 4), where eight times as many trees in the 20–29 DBH class were obscured by trees in crown exposure class 5, as those in the 40–49 DBH class. The relationship between crown length or crown area and the total number of tree stems obscured is provided in Fig. 5A and B, showing a minimum and maximum of 1–18 obscured tree stems. The nadir-viewable crown area and the crown exposure class had, as expected, a strong negative relationship with 100% of crown position 5 being visible, while only 55% and 60% of crown area in positions 3 and 4 was visible, respectively. Crown exposure classes 1 and 2 were almost entirely obscured by other crowns (Table 3).

Correction equations necessary to convert remotely sensed data to field-based structural data are illustrated in Fig. 5, and the equations are provided in Appendix C. Significant relationships were identified between crown length and crown area and the number of obscured trees (Fig. 5A and B). Additional relationships were derived to relate crown length and area to basal area and biomass for both the nadir-visible trees and including the obscured trees (Fig. 5C–F). Basal area and biomass estimates increased by 30–50%, largely depending on the crown area of the exposed tree crowns, when we included all obscured trees in comparison to calculations based only on nadir-visible trees.

A total of 370 tree crowns were identified using the remote sensing methodology, although there were 531 tree crowns measured in the field (Fig. 6). The abundance of remotely identified trees in study plots 1, 3 and 4 represented less than half the trees identified in the field, while remote tree stem counts in study plot 2 was almost three times higher than the trees identified in the field (Table 1).

The remotely sensed circle and polygon delineation approach identified 70 and 108 trees having DBH < 20 cm, respectively. In the field trees with DBH < 20 cm were not included (Fig. 7A). These same approaches identified far fewer tree individuals in the 20–29 DBH class, with 43 and 59 trees identified using the circle and polygon approach, versus 249 trees identified in this class in the field, resulting in significantly different distributions. The remote sensing approaches identified trees with DBH values up to 110 cm, but identified few greater than this threshold (Fig. 7A). While crown areas from both the remotely sensed circle and polygon approaches had significantly different (with greater and lower areas, respectively; see Table 6) crown area distributions from those of field measurements, the DBH distributions quantified from these areas do not differ between the remotely sensed polygon approach and field measurements (Table 7). While the nadir-visible biomass equations on the remote sensing circle approach did not significantly differ from field measurements, the polygon approach did so. When the corrected biomass equation, accounting for obscured trees, was used, stand biomass estimates from the remotely sensed circle approach significantly differed, while the polygon approach did not, from the field values (Table 7, Appendix C).

Direct comparisons between field-delineated tree crowns and remotely sensed crown polygons was conducted for 21, 21 and 42 trees for crown exposure classes 3, 4 and 5, respectively. Trees in exposure classes 1 and 2 were not used, as by definition, they are obscured from nadir-viewing remote sensors. Seventy-four percent of field-delineated tree crowns in crown exposure 5 had automated detections centered within them, while only 38% of crowns in exposure class 4 and 3 were detected via our remote sensing methodology. A significant linear relationship existed between emergent tree biomass calculated from field-measured variables and the biomass estimated from remotely identified crown polygons (remotely sensed polygon corrected biomass = $2.22 + 0.54 \times$ field biomass; $r^2 = 0.42$, $p < 0.0001$), while non-significant relationships were found in exposure classes 3 and 4. Significant positive relationships were found between field-delineated crown areas and the number of remote circle and polygon detections within a given crown area (for crown exposure class 3: RS detections = $0.13 + 0.006 \times$ field area; $r^2 = 0.68$, $p < 0.0001$; for class 4: RS detections = $-0.11 + 0.007 \times$ field area; $r^2 = 0.46$, $p < 0.015$; and for crown exposure class 5: RS detection = $0.496 + 0.003 \times$ field crown area; $r^2 = 0.53$, $p < 0.0001$).

4. Discussion

Biomass inventories are needed to track forest carbon dynamics. High-resolution satellite imagery is starting to

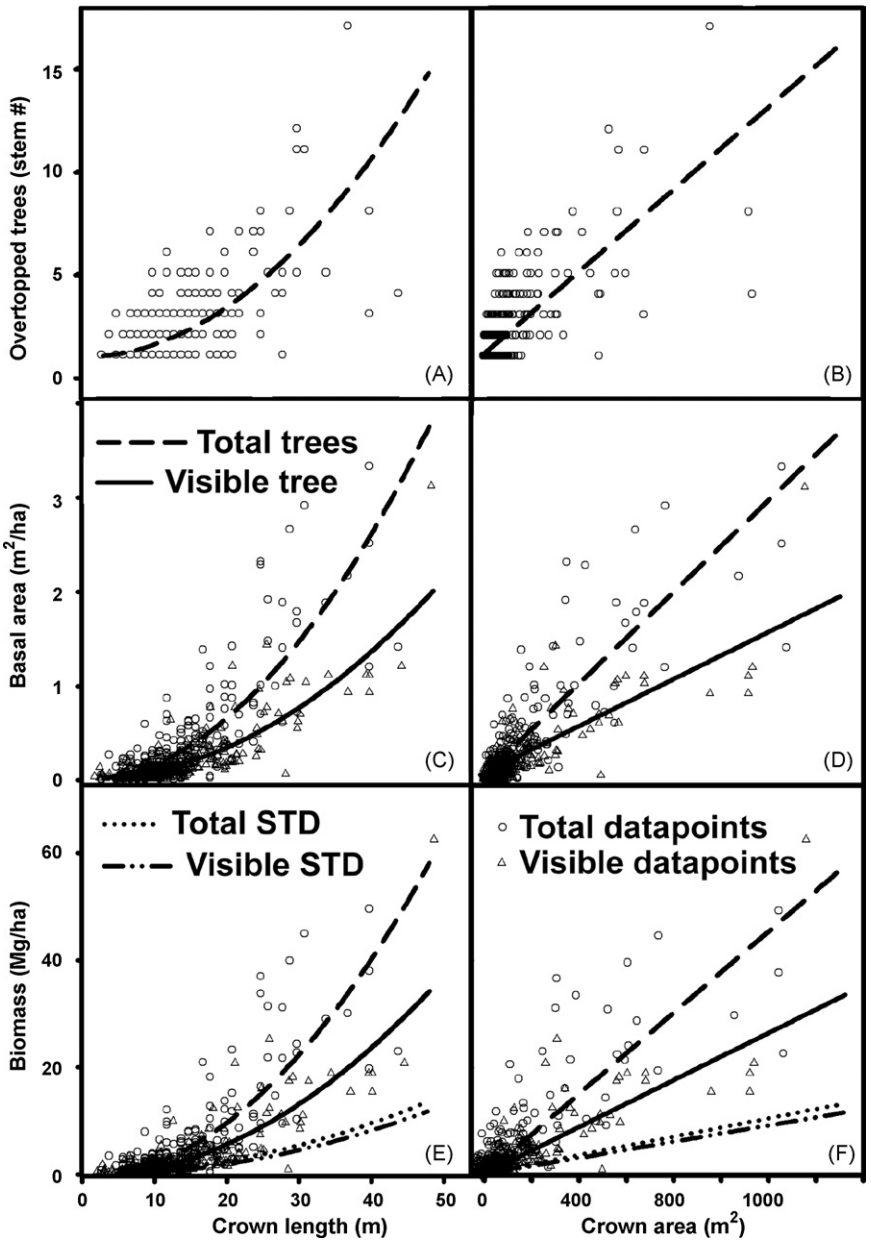

Fig. 5. Correction factors for obscured understory trees for: tree abundance (A and B), basal area (C and D) and biomass (E and F) for trees with DBH $\geq$ 20 cm using crown length and crown area. Equations are provided in Appendix C. STD represents the standard deviation of the six biomass equations used in the analysis and is provided to indicate the potential error in the biomass estimation.

enable structural analysis of tropical forests over large areas, but we lack an understanding of how the spatial distribution of tropical forest biomass links to remote sensing. Furthermore, the high diversity of tree species present in tropical forests adds to their structural and spectral complexity, impeding many remote-sensing approaches. An increased understanding of how tree species diversity is distributed within the forest could assist in the development of methods which take advantage of this diversity. To interpret results from remote sensing, it is first necessary to understand how forest biomass and tree species diversity are horizontally and vertically distributed.

4.1. Spatial distribution of forest biomass

The highest tree abundance was found in the smallest DBH classes (Table 2), while basal area and biomass were more or less equally distributed among the different size classes. The distribution of stem abundance observed across DBH categories is typical of tropical forests (Cummings et al., 2002). Our vertical crown exposure data showed that the highest values of basal area, DBH, and total height occurred within emergent trees (Table 3), which encompassed about 58% of the total forest biomass found in our study sites, but represent only 20% of the 531 trees in our study plots. Other studies have highlighted large quantities of

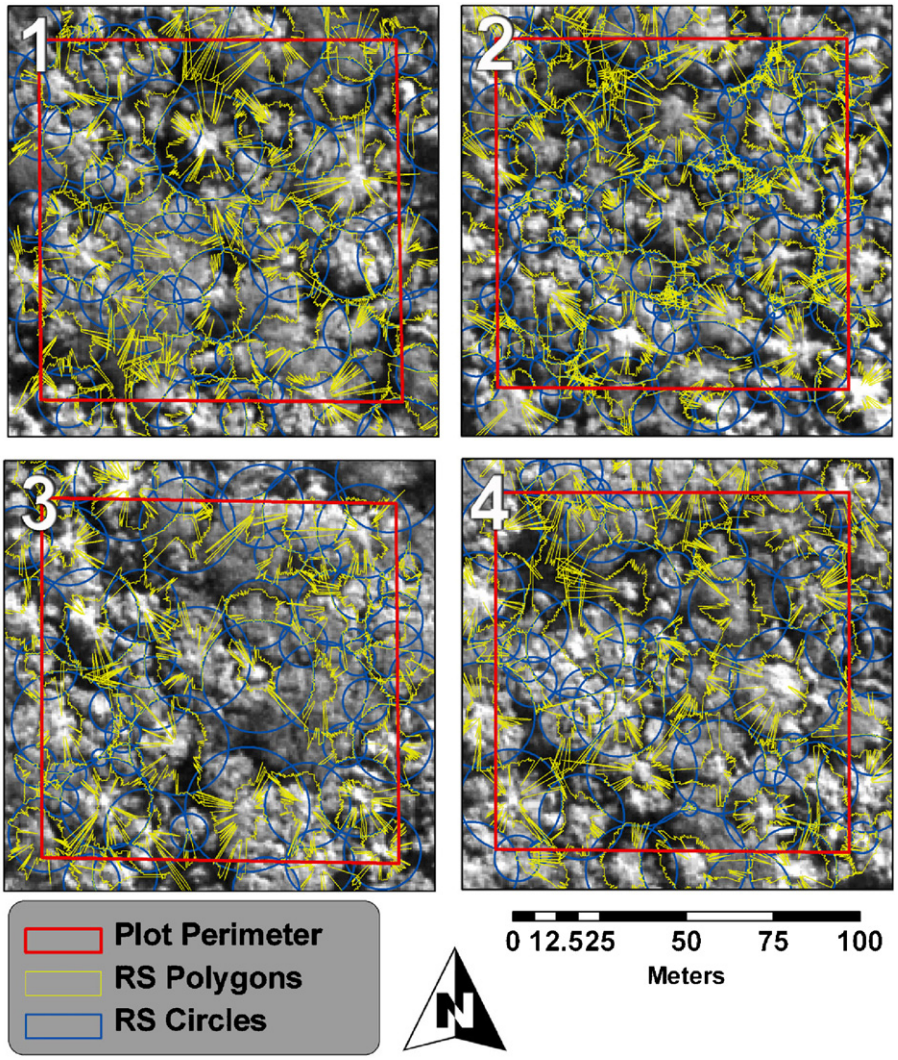

Fig. 6. Automated circle and polygon crown delineations in study plots 1–4 (top left corner) overlaid on the panchromatic Quickbird satellite image.

biomass being stored in emergent trees (Keller et al., 2001), but noted that emergent trees were quite rare.

An analysis across the Amazon showed that dry season length was positively correlated with percentage biomass stored in trees with diameters ≥50 cm, with a maximum storage of 41–45% biomass stored above that DBH threshold (Vieira et al., 2004). Our results are higher than these, and may be partly explained by the fact that our study location

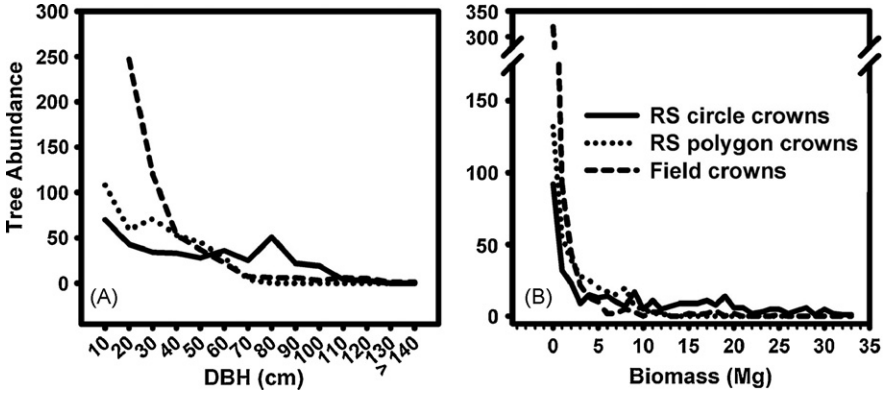

Fig. 7. Abundance of trees by 10 cm DBH classes (a) and biomass (Mg) (b). The *x*-axis labels represent the lower limit of the size class. Biomass derived using remote sensing circle and polygon approaches is calculated using the corrected biomass equation incorporating obscured tree stems provided in Appendix C.

Table 6
Remote sensing (RS) and field delineated crown area (m^2), tree diameter (cm) and individual tree biomass (Mg) statistics

	Min.	Max.	Mean	S.D.
RS polygon crown area	1.13	333	75.1	78.9
RS circle crown area	1.13	1052	234.3	240.9
Field crown area	0[a]	1524	90.8	157.4
RS polygon DBH	11.5	73.3	33.8	17.2
RS circle DBH	11.5	124.4	53.6	30.6
Field DBH	11.0	200.0	37.0	21.1
RS polygon biomass	0.06	6.86	1.00	1.47
RS circle biomass	0.06	21.52	3.02	4.52
Field biomass	0.08	62.55	1.95	0.08

[a] No crown area present due to damage.

Table 7
Kolmogorov–Smirnov comparison *D* values between remote sensing (circle and polygon approaches) and field measurement distributions across the four 1-ha study plots

	RS circle vs. RS polygon	RS circle vs. field	RS polygon vs. field
Crown area (m^2)	0.5366***	0.3659**	0.3902**
DBH (cm)	0.3571 ns	0.3571 ns	0.4286 ns
Remotely visible biomass (Mg)	0.3889**	0.2500 ns	0.3333*
Corrected biomass (Mg)	0.611***	0.5278***	0.1667 ns

*$p < 0.05$; **$p < 0.01$; ***$p < 0.001$.

has a more pronounced dry season than any of the study sites addressed in the previous analysis. An alternate explanation would be the past land-use history in our study forest. Previous research has shown extensive distributions of anthropogenic terra-preta soil containing 500-year-old pottery shards (Paz, 2003), suggesting that we may be seeing the remnant composition and forest structure of this period, especially as these trees may be many hundreds of years old (Chambers et al., 1998). Many of the largest trees in the forest are *Ficus* spp., known to be shade intolerant. These large trees show very little recruitment in the understory, implying that they became established under very different climatic conditions or disturbance regimes than at present or are the result of historical management practices. The significantly greater spatial clumping of emergent trees, as compared to all other crown exposure classes (Fig. 2), may be related to either past land-use history or the existence of fine-scale topo-edaphic gradients within our study plots (Vroomans, 2003; Paoli et al., 2008). The greater separation distance between understory tree stems in exposure class 1 may be explained by exclusion of tree stems smaller than our ≥20 cm DBH threshold.

Emergent trees had longer crown length and crown width, and consequently larger crown area, than trees in the other crown exposure classes (Table 3), likely due to the fact that trees expand their crowns when they reach the canopy of tropical forests (O'Brien et al., 1995; Poorter et al., 2005, 2006). The lack of correlation between DBH class and biomass resulted from larger DBH trees occurring at lower densities (Table 2).

4.2. Spatial distribution of forest diversity

Trees in the emergent tree class represented 59% of all species found in our study area, although they composed only 20% of the 531 trees >20 cm DBH within our study plots. When considering the three exposure classes likely viewable to a nadir remote sensor (exposure classes 5-3), we found that 86% of all tree species ≥20 cm DBH were represented. Thus the vast majority of tropical forest tree diversity for stems ≥20 cm DBH could be quantified and monitored using nadir-viewing remote sensing techniques, such as the ones used in this study and in a study carried out in Hawaiian tropical forests (Carlson et al., 2007).

4.3. Linking field and remote sensing measurements

Since the emergent trees had the largest canopies and the tallest mean height, they obscured the largest number of understory trees (Fig. 4). Consequently, emergent trees obscure the understory biomass from nadir-viewing remote sensors, which resulted in an underestimation of biomass. It was possible with the first round of correction equations developed in this study to include the obscured trees so that the corrected biomass calculation did not differ significantly from the biomass estimations using field data (Table 7). These correction equations are inherently site-specific; consequently, the development of these types of spatial equations needs to be conducted for the large variety of forest types and forest ages found throughout the tropics to accurately determine full stand biomass from remote sensing. Forests having a greater stature or increased tree diversity would likely have greater standing biomass and diversity masked by overstory tree crowns. Understanding how the spatial distribution of biomass and tree species diversity differs among forest biomes and along climatic gradients, however, has not been well studied and is a topic we are currently investigating.

The automated crown delineation approach worked well at the community scale, although the circular crown measurement approach tended to over-estimate tree crown areas for smaller crowns, while erroneously dissecting larger crowns into multiple individuals. When remotely sensed tree crown area was converted to DBH using our allometric relationships, we found we had identified many tree individuals below our field diameter threshold of 20 cm. This is not unexpected, as our DBH threshold (≥20 cm DBH) meant that many small but nadir-visible tree crowns were not delineated and mapped in the field. This is apparent in the large open areas in Fig. 3 as compared with Fig. 6, where smaller crowns have been automatically delineated throughout the plots. Consequently, we suggest that future studies use crown exposure class instead of DBH to define sample trees, although we recognize the large (and sometimes infeasible) difficulties associated with such a survey. Even considering

these differences, however, biomass estimated via remote sensing did not have significantly different distributions of biomass from those mapped in the field after using our equations developed to correct for obscured trees. Our corrected biomass equation resulted in an increase of remotely estimated tree biomass of 30–50%, depending on the crown area. The utility of a crown-dependent conversion equation is highlighted in our clumping analysis, where it is shown that the forest in our study area is not homogeneous throughout the landscape, but rather varies in structure at fine spatial scales. Relationships between topography and forest structure and diversity, among other factors, have been identified within our study area (Vroomans, 2003) and warrant further investigation at larger scales via remote sensing.

Results from our remote sensing approaches were mixed at the tree-to-tree scale. Although the crown delineation program applied in this study captured many of the textural features of the Quickbird image, most of the larger emergent canopies were segmented into smaller crowns, while some smaller trees visually appeared to be merged. Our remote sensing analyses indicate that individual tree crowns are not easily quantified due to the highly heterogeneous matrix of shadows, intrinsic crown characteristics at the species level, multiple sub-crowns within a single tree, and canopy gap disturbances. Whether such problems would be exacerbated by the greater diversity and/or higher standing biomass typical of some tropical forests (Palace et al., 2008) would depend on the spatial distribution of tree diversity and biomass in those forests. For example, biomass uncertainty could be reduced in forests having fewer understory trees, such as some found in South East Asian. Our results do show, however, that even in these forests, which are noticeably more structurally heterogeneous than those in other areas of the Amazon, there is great potential for the approach to document larger-scale patterns in community structure and biomass. Further improvements to this technique will require: (1) a greater understanding of the spatial distribution of tree diversity and biomass in a variety of forest types, (2) the inclusion of spectral data to differentiate between adjacent tree crowns, and (3) improvement of the crown edge detection algorithm.

5. Conclusions

Improved understanding of the spatial distribution of forest species diversity and biomass will aid in the development of remote sensing approaches capable of rapidly and cost-effectively quantifying these factors over large areas of tropical forest. Such data are necessary for fine-scale forest management, biomass assessments, and conservation planning of tropical forests. In our study of a lowland moist semi-deciduous tropical forest in Bolivia, the upper-canopy and often emergent trees comprised the majority of the tree diversity and biomass. Trees with crowns visible to nadir remote sensors represented 86% of all tree species $\geq$20 cm DBH in our study plots. Emergent trees obscured many subordinate trees with DBH $\geq$ 20 cm, resulting in 30–50% of the forest biomass being hidden from nadir (e.g., satellite) view. Our allometric equations were specifically developed to link the portion of the forest that was remotely sensible to field parameters. Our subsequent correction equations allowed us to derive aboveground forest biomass, basal area, and tree density from only those tree crowns visible to the Quickbird satellite sensor. Although the automated crown detection algorithm employed here requires continued development, it did show promise for delivering high-resolution maps of forest structure. Our future efforts will focus on ways to improve both the satellite sensing approaches via enhanced algorithms and inclusion of spectral information, and their linkage to the full complexity of tropical forest diversity and biomass in three dimensions.

Acknowledgements

We thank the Instituto Boliviano de Investigación Forestal (IBIF) for field and logistical assistance and La Chonta Ltda. for allowing us access to their forest concession. We thank Don Ricardo Mendez for help with data collection. We thank Angelica Almeyda for helpful comments and logistical support. This work was supported by NASA LBA-ECO grant NNG06GE32A (LC-33) and the Carnegie Institution.

Appendix A

Aboveground biomass equations found in the literature (kg). ρ = wood density (g/cm^3), DBH = bole diameter at breast height (1.3 m; cm), and H = total tree height (m).

ID	Equation	References
A	$M = 42.69 + (-12.8) \times \mathrm{DBH} + 1.242 \times \mathrm{DBH}^2$	Brown (1997)
B	$M = \exp[-2.134 + 2.53 \times \ln(\mathrm{DBH})]$	Brown (1997)
C	$M = 0.6 \times (4.06 \times \mathrm{DBH}^{1.76})$	Araujo et al. (1999)
D	$M = 1000 \times 0.6 \times \exp[3.323 + 2.546 \times \ln(\mathrm{DBH}/1000)]$	Carvalho et al. (1988)
E	$M = 0.112 \times (\rho \times \mathrm{DBH}^2 \times \mathrm{H})^{0.916}$	Chave et al. (2005)
F	$\mathrm{M} = 0.0509 \times (\rho \times \mathrm{DBH}^2 \times \mathrm{H})$	Chave et al. (2005)

Appendix B. Bivariate power regressions between all forest structural variables. R values are presented in parentheses and P value significance is provided as: * = $p < 0.05$, ** = $p < 0.01$, *** = $p < 0.001$, NS = non-significant, following each equation.

Variable	Crown position	Tree total (TT)	Depth (m) (*D*)	Length (m) (*L*)	Width (m) (*W*)	Area (m^2) (*A*)	Volume (m^3) (*V*)
DBH (cm)	5	$=29.2 + 0.001 \times TT^{3}(0.58)$***	$=29.27 + 0.81 \times D^{1.5}(0.37)$***	$=10.55 + 2.97 \times L(0.74)$***	$=21.96 + 3.02 \times W(0.68)$***	$=16.35 + 3.44 \times A^{0.5}(0.73)$***	$=26.12 + 0.95 \times V0.5(0.71)$***
	4	$=28.21 + 0.001 \times TT^{3}(0.35)$***	$=33.85 + 0.006 \times D^{3}(0.30)$***	$=24.06 + 0.10 \times L^{2}(0.58)$***	$=25.59 + 0.198 \times W(0.59)$***	$=31.43 + 0.009 \times A^{1.5}(0.65)$***	$=31.78 + 0.015 \times V(0.61)$***
	3	$=12.38 + 0.97 \times TT(0.23)$***	$=20.5 + 1.58 \times D(0.17)$***	$=11.60 + 1.94 \times L(0.47)$***	$=16.22 + 2.23 \times W(0.35)$***	$=23.91 + 0.11 \times A(0.43)$***	$=19.89 + 0.74 \times V^{0.5}(0.41)$***
	2	$=21.00 + 0.001 \times TT^{3}(0.41)$***	$=23.74 + 0.08 \times D^{2}(0.15)$***	$=15.91 + 1.26 \times L(0.27)$***	$=23.57 + 0.03 \times W^{2.5}(0.44)$***	$=24.84 + 0.001 \times A^{2}(0.53)$***	$=24.52 + 0.001 \times V^{1.5}(0.56)$***
	1	$=15.17 + 0.46 \times TT(0.19)$***	$=21.51 + 0.02 \times D^{2.5}(0.13)$**	$=19.12 + 0.47 \times L(0.08)$*	ns	ns	$=22.29 + 0.0004 \times V^{1.5}(0.10)$**
	All	$=23.42 + 0.001 \times TT^{3}(0.56)$***	$=29.76 + 0.008 \times D^{3}(0.35)$***	$=4.13 + 2.92 \times L(0.65)$***	$=11.55 + 3.29 \times W(0.62)$***	$=7.62 + 3.60 \times A^{0.5}(0.66)$***	$=17.67 + 0.94 \times V^{0.51}(0.67)$***
Height (m)							
First branch (FB)	5	$=-4.70 + 3.21 \times TT^{0.5}(0.33)$***	$=10.15 + 0.19 \times D(0.05)$*	ns	ns	ns	ns
	4	$=-3.57 + 2.96 \times TT^{0.5}(0.28)$***	$=9.94 + 0.008 \times D^{2}(0.03)$***	ns	ns	ns	ns
	3	$=-21.54 + 14.75 \times TT^{0.24}(0.41)$***	$=6.15 + 0.32 \times D(0.08)$**	ns	ns	ns	ns
	2	$=-19.70 + 12.18 \times TT^{0.29}(0.39)$***	ns	ns	ns	ns	ns
	1	$=-6.08 + 3.41 \times TT^{0.5}(0.39)$***	ns	ns	ns	ns	ns
	All	$=-6.17 + 3.44 \times TT^{0.5}(0.45)$***	$=6.87 + 0.36 \times D(0.12)$***	$=7.66 + 0.17 \times L(0.06)$***	$=8.8 + 0.67 \times W(0.01)$*	$=7.89 + 0.20 \times A^{0.5}(0.05)$***	$=9.14 + 5.2e\text{-}04 \times V(0.05)$***
Canopy base (CB)	5	$=-10.26 + 5.20 \times TT^{0.5}(0.69)$***	$=8.89 + 2.37 \times D^{0.5}(0.14)$***	$=12.78 + 0.30 \times L(0.28)$***	$=14.07 + 0.29 \times W(0.23)$***	$=13.43 + 0.33 \times A^{0.5}(0.26)$***	$=4.47 + 5.51 \times V0.13(0.28)$***
	4	$=-7.03 + 4.43 \times TT^{0.5}(0.59)$***	$=12.14 + 0.25 \times D(0.06)$*	$=10.71 + 0.30 \times L(0.11)$***	$=11.46 + 0.35 \times W(0.09)$***	$=10.88 + 0.40 \times A^{0.5}(0.11)$***	$=11.0 + 0.42 \times V0.35(0.10)$***
	3	$=-7.50 + 4.50 \times TT^{0.5}(0.70)$***	$=8.86 + 0.44 \times D(0.15)$***	$=8.28 + 0.28 \times L(0.15)$***	$=8.9 + 0.41 \times W(0.14)$***	$=10.46 + 0.02 \times A(0.14)$***	$=9.42 + 0.15 \times V0.5(0.19)$***
	2	$=-9.95 + 5.08 \times TT^{0.5}(0.63)$***	ns	$=9.01 + 0.26 \times L(0.06)$**	ns	$=11.06 + 6.54e\text{-}06 \times A^{2}(0.08)$***	$=11.15 + 1.59e\text{-}09 \times V3(0.07)$**
	1	$=0.70 + 0.57 \times TT(0.67)$***	ns	ns	ns	ns	ns
	All	$=-9.35 + 4.94 \times TT^{0.5}(0.74)$***	$=9.27 + 0.53 \times D(0.20)$***	$=8.54 + 0.42 \times L(0.29)$***	$=9.75 + 0.45 \times W(0.25)$***	$=9.04 + 0.51 \times A0.5(0.27)$***	$=8.24 + 0.78 \times V0.32(0.29)$***
Tree total (TT)	5		$=-1.67 + 9.8 \times D^{0.5}(0.69)$***	$=18.56 + 0.66 \times L(0.50)$***	$=12.53 + 5.06 \times W^{0.5}(0.46)$***	$=19.94 + 0.75 \times A^{0.5}(0.48)$***	$=1.14 + 10.01 \times V^{0.15}(0.64)$***
	4		$=12.12 + 1.37 \times D(0.67)$***	$=14.38 + 0.77 \times L(0.27)$***	$=15.98 + 0.97 \times W(0.23)$***	$=14.57 + 1.07 \times A^{0.5}(0.27)$***	$=11.34 + 1.61 \times V^{0.34}(0.52)$***
	3		$=8.86 + 1.57 \times D(0.69)$***	$=10.94 + 0.76 \times L(0.30)$***	$=12.13 + 0.99 \times W(0.29)$***	$=11.15 + 1.05 \times A^{0.5}(0.32)$***	$=12.58 + 0.41 \times V^{0.5}(0.52)$***
	2		$=10.75 + 1.22 \times D(0.44)$***	$=12.22 + 0.63 \times L(0.19)$***	$=14.37 + 0.59 \times W(0.10)$***	$=15.59 + 0.48 \times A(0.16)$***	$=12.53 + 0.42 \times V^{0.5}(0.35)$***
	1		$=8,93 + 1.39 \times D(0.53)$***	ns	ns	ns	$=12.14 + 0.42 \times V^{0.5}(0.26)$***
	All		$=9.26 + 1.65 \times D(0.71)$***	$=11.57 + 0.89 \times L(0.46)$***	$=14.07 + 0.97 \times W(0.41)$***	$=12.61 + 1.09 \times A(0.45)$***	$=5.96 + 3.55 \times V^{0.26}(0.63)$***
Crown							
Depth (*D*)	5			$=5.15 + 0.33 \times L(0.41)$***	$=6.47 + 0.32 \times W(0.37)$***	$=5.80 + 0.37 \times A^{0.5}(0.40)$***	$=2.31 \times V^{0.22}(0.63)$***
	4			$=3.28 + 0.43 \times L(0.23)$***	$=4.03 + 0.55 \times W(0.20)$***	$=6.13 + 0.026 \times A(0.23)$***	$=-3.39 + 3.09 \times V^{0.23}(0.65)$***
	3			$=2.14 + 0.40 \times L(0.29)$***	$=2.78 + 0.52 \times W(0.28)$***	$=2.23 + 0.56 \times A^{0.5}(0.31)$***	$=2.78 + 0.23 \times V^{0.5}(0.58)$***
	2			$=2.86 + 0.33 \times L(0.17)$***	$=3.70 + 0.25 \times W(0.13)$***	$=3.03 + 0.43 \times A^{0.5}(0.17)$***	$=2.27 + 0.28 \times V^{0.5}(0.52)$***
	1			$=3.82 + 0.24 \times L(0.08)$*	$=3.65 + 0.41 \times W(0.14)$***	$=2.8 + 0.51 \times A^{0.5}(0.20)$***	$=1.99 + 0.32 \times V^{0.5}(0.55)$***
	All			$=2.71 + 0.42 \times L(0.39)$***	$=3.85 + 0.46 \times W(0.35)$***	$=3.14 + 0.52 \times A^{0.5}(0.39)$***	$=1.56 \times V^{0.28}(0.68)$***
Length (*L*)	5				$=4.02 + 0.999 \times W(0.89)$***	$=0.31 + 1.19 \times A^{0.5}(0.94)$***	$=5.56 + 0.307 \times V^{0.5}(0.91)$***
	4				$=2.83 + 1.127 \times W(0.71)$***	$=0.91 + 1.28 \times A^{0.5}(0.90)$***	$=1.86 \times V^{0.31}(0.71)$***
	3				$=2.79 + 1.088 \times W(0.68)$***	$=1.14 + 1.25 \times A^{0.5}(0.86)$***	$=4.55 + 0.36 \times V^{0.5}(0.78)$***
	2				$=3.07 + 0.978 \times W(0.63)$***	$=1.02 + 1.23 \times A^{0.5}(0.86)$***	$=3.57 + 0.42 \times V^{0.5}(0.74)$***
	1				$=3.29 + 0.949 \times W(0.51)$***	$=1.04 + 1.25 \times A^{0.5}(0.80)$***	$=3.51 + 0.42 \times V^{0.5}(0.65)$***
	All				$=3.08 + 1.05 \times W(0.83)$***	$=1.41 + 1.20 \times A^{0.5}(0.94)$***	$=1.74 \times V^{0.32}(0.88)$***

Appendix B (*Continued*)

Variable	Crown position	Tree total (TT)	Depth (m) (*D*)	Length (m) (*L*)	Width (m) (*W*)	Area (m^2) (*A*)	Volume (m^3) (*V*)
Width (*W*)	5					$=-1.37+1.10\times A^{0.5}(0.98)^{***}$	$=2.08+0.29\times V^{0.5}(0.91)^{***}$
	4					$=-0.42+0.98\times A^{0.5}(0.94)^{***}$	$=1.04\times V^{0.34}(0.73)^{***}$
	3					$=-0.46+0.99\times A^{0.5}(0.93)^{***}$	$=2.34+0.28\times V^{0.5}(0.82)^{***}$
	2					$=-0.62+1.03\times A^{0.5}(0.92)^{***}$	$=1.67+0.34\times V^{0.5}(0.73)^{***}$
	1					$=-1.04+1.26\times A^{0.5}(0.71)^{***}$	$=1.46+0.34\times V^{0.5}(0.74)^{***}$
	All					$=-0.9+1.06\times A^{0.5}(0.97)^{***}$	$=0.78\times V^{0.4}(0.88)^{***}$
Area (*A*)	5						$=8.37+0.60\times V^{0.79}(0.94)^{***}$
	4						$=8.22+1.01\times V^{0.70}(0.88)^{***}$
	3						$=1.42\times V^{0.68}(0.93)^{***}$
	2						$=1.19\times V^{0.71}(0.82)^{***}$
	1						$=1.26\times V^{0.69}(0.81)^{***}$
	All						$=0.81\times V^{0.75}(0.93)^{***}$

N is greater than 128, 149, 178, 152, 63 (670 total) for crown positions 5-1 and all, respectively.

Appendix C.

Correction equations for converting nadir top-of-canopy estimations based on the single visible tree crown (RS) to corrected forest biomass incorporating obscured tree stems ≥20 cm DBH (FB). *p*-Values are provided following each equation and r^2 values are provided in parentheses. $^{*}p < 0.05$, $^{**}p < 0.01$, $^{***}p < 0.001$. NS = non-significant ($n \geq 314$).

Variables	Crown Length (m)	Crown area (m^2)
Obscured trees (stem#)	$FB = 1.02 + 0.006 \times L^2(0.56)^{***}$	$FB = 1.17 + 0.01 \times A(0.62)^{***}$
Basal area (m^2/ha)	$FB = 40.21 + 16.3 \times L^2(0.66)^{***}$ $RS = 161.6 + 8.65 \times L^2(0.74)^{***}$	$FB = 486.67 + 24.31 \times A(0.69)^{***}$ $RS = 449.4 + 12.47 \times A(0.72)^{***}$
Biomass (Mg/ha)	$FB = -562.09 + 25.49 \times L^2(0.62)^{***}$ $RS = -420.27 + 14.17 \times L^2(0.70)^{***}$	$FB = 148.37 + 37.92 \times A(0.65)^{***}$ $RS = 55.63 + 20.4 \times A(0.67)^{***}$

References

Araujo, T.M., Higuchi, N., Carvalho Jr., J.A., 1999. Comparison of formulae for biomass content determination in a tropical rain forest site in the state of Para, Brazil. For. Ecol. Manage. 117, 43–52.

Asner, G.P., Palace, M., Keller, M., Pereira Jr., R., Silva, J.N.M., Zweede, J.C., 2002. Estimating canopy structure in an Amazon forest from laser range finder and IKONOS satellite observations. Biotropica 34, 483–492.

Baker, T.R., Phillips, O.L., Malhi, Y., Almeida, S., Arroyo, L., Di Fiore, A., Erwin, T., Killeen, T.J., Laurance, S.G., Laurance, W.F., Lewis, S.L., Lloyd, J., Monteagudo, A., Neill, D.A., Patino, S., Pitman, N.C.A., Silva, J.N.M., Martinez, R.V., 2004. Variation in wood density determines spatial patterns in Amazonian forest biomass. Global Change Biol. 10, 545–562.

Brokaw, N., 1985. Gap-phase regeneration in a tropical forest. Ecology 66, 682.

Brown, S., 1997. Estimating Biomass and Biomass Change of Tropical Forests, A Primer. FAO Forestry Paper 134. United Nations Food and Agriculture Organization, Rome, 55 pp.

Calla, S.A., 2003. Arquelogía de ''La Chonta''. BOLFOR, Santa Cruz, Bolivia, 53 pp.

Carlson, K.C., Asner, G.P., Hughes, R.F., Ostertag, R., Martin, R.E., 2007. Hyperspectral remote sensing of canopy biodiversity in Hawaiian lowland rainforests. Ecosystems 10, 536–549.

Carvalho Jr., J.A., Higuchi, N., Araujo, T.M., Santos, J.C., 1988. Combustion completeness in a rainforest clearing experiment in Manaus, Brazil. J. Geophys. Res. 103, 13199–13915.

Chambers, J., Higuchi, N., Schimel, N., 1998. Ancient trees in the Amazon. Nature 391, 135–136.

Chambers, J.Q., dos Santos, J., Ribeiro, R.J., Higuchi, N., 2000. Tree damage, allometric relationships, and above-ground net primary production in central Amazon forest. For. Ecol. Manage. 5348, 1–12.

Chave, J., Andalo, C., Brown, S., Cairns, M.A., Chambers, J.Q., Eamus, D., Folster, H., Fromard, F., Higuchi, N., Kira, T., Lescure, J.-P., Nelson, B.W., Ogawa, H., Puig, H., Riera, B., Yamakura, T., 2005. Tree allometry and improved estimation of carbon stocks and balance in tropical forests. Oecologia 145, 87–99.

Clark, D.A., Clark, D.B., 1992. Life history diversity of canopy and emergent trees in a neotropical rain forest. Ecol. Monogr. 62, 315–344.

Clark, D.B., Castro, C.S., Alvarado, L.D.A., Reed, J.M., 2004. Quantifying mortality of tropical rain forest trees using high-spatial-resolution satellite data. Ecol. Lett. 7, 52–59.

Cordero, W., 2000. Determinación del daño causado por los incendios forestales ocurridos en los departamentos de Santa Cruz-Beni en los meses de agosto y septiembre de 1999. Informe Final. Corporación Andina de Fomento, Proyecto BOLFOR, & Geosystems. Santa Cruz, Bolivia, 43 pp.

Cummings, D.L., Boone Kauffman, J., Perry, D.A., Flint Hughes, R., 2002. Aboveground biomass and structure of rainforests in the southwestern Brazilian Amazon. For. Ecol. Manage. 163, 293–307.

Dauber, E., Teran, J., Guzman, R., 2000. Estimaciones de biomasa y carbono en bosques naturales de Bolivia. Superintendencia Forestal, Santa Cruz, Bolivia, 62 pp.

Drake, J.B., Dubayah, R.O., Clark, D.B., Blair, J.B., Hofton, M.A., Chazdon, R.L., Weishampel, J.F., Prince, S., 2002. Estimation of tropical forest structural characteristics using large-footprint lidar. Remote Sens. Environ. 79, 305–319.

Gould, K.A., Fredericksen, T.S., Morales, F., Kennard, D., Putz, F.E., Mostacedo, B., Toledo, M., 2002. Post-fire tree regeneration in lowland Bolivia, implications for fire management. For. Ecol. Manage. 165, 225–234.

Guariguata, M.R., Chazdon, R.L., Denslow, J.S., Dupuy, J.M., Anderson, L., 1997. Structure and floristics of secondary and old-growth forest stands in lowland Costa Rica. Plant Ecol. 132, 107–120.

Hansen, A.J., Spies, T.A., Swanson, F.J., Ohmann, J.L., 1991. Conserving biodiversity in managed forests, lessons from natural forests. BioScience 41, 382–392.

Keller, M., Palace, M., Hurtt, G., 2001. Biomass estimation in the Tapajos National Forest, Brazil, Examination of sampling and allometric uncertainties. For. Ecol. Manage. 154, 371–382.

Kuppers, M., 1989. Ecological significance of aboveground architectural patterns in woody plants. A question of cost-benefit relationships. Trends Ecol. Evol. 4, 375–379.

O'Brien, S.T., Hubbell, S.P., Spiro, P., Condit, R., Foster, R.B., 1995. Diameter, height, crown, and age relationships in eight neotropical tree species. Ecology 76, 1926–1939.

Palace, M., Keller, M., Asner, G.P., Hagen, S., Braswell, B., 2008. An analysis of Amazonian forest structure using an automated tree crown detection algorithm and IKONOS imagery. Biotropica 40, 141–150.

Paoli, G.D., Curran, L.M., Slik, J.W.F., 2008. Soil nutrients affect spatial patterns of aboveground biomass and emergent tree density in southwestern Borneo. Oecologia 155, 287–299.

Paz, C., 2003. Forest-use History and the Soils and Vegetation of a Lowland Forest in Bolivia. University of Florida, Gainesville, Florida, 67 pp.

Peña-Claros, M., Peters, E.M., Justianiano, M.J., Bongers, F., Blate, G.M., Fredericksen, T.S., Putz, F.E., 2008. Regeneration of commercial tree species following silvicultural treatments in a moist tropical forest. For. Ecol. Manage. 255, 1283–1293.

Phillips, O.L., Malhi, Y., Higuchi, N., Laurance, W.F., Nunes, P.V., Vasquez, R.M., Laurence, S.G., Ferreira, L.V., Stern, M., Brown, S., Grace, J., 1998. Change in the carbon balance of tropical forests, evidence from long-term plots. Science 282, 439–442.

Poorter, L., Bongers, F., Sterck, F.J., Woll, H., 2005. Beyond the regeneration phase, differentiation of height-light trajectories among tropical tree species. J. Ecol. 93, 256–267.

Poorter, L., Bongers, L., Bongers, F., 2006. Architecture of 54 moist-forest tree species, traits, trade-offs, and functional groups. Ecology 87, 1289–1301.

Slik, J.W.F., 2006. Estimating species-specific wood density from the genus average in Indonesian trees. J. Trop. Ecol. 22, 481–482.

Superintendencia Forestal, 2002. Informe Anual Gestión 2002. Santa Cruz, Bolivia, 45 pp.

Vieira, S., Camargo, P.B., Selhorst, D., Silva, R., Hutyra, L., Chambers, J.Q., Brown, I.F., Higuchi, N., Santos, J., Wofsy, S., Trumbore, S.E., Martinelli, L.A., 2004. Forest structure and carbon dynamics in Amazonian tropical rain forest. Oecologia 40, 468–479.

Vroomans, V., 2003. Topografía de las parcelas permanentes en la concesión forestal La Chonta y su efecto en la vegetación. Documento Tecnico# 156/2003. Proyecto BOLFOR, Santa Cruz, Bolivia, 77 pp.

Whitmore, T.C., 1978. Gaps in the forest canopy. In: Tomlinson, P.B., Zimmerman, M. (Eds.), Tropical Trees as Living Systems. Cambridge University Press, New York, pp. 639–655.

Whitmore, T.C., 1989. Canopy gaps and the two major groups of forest trees. Ecology 70, 536.